J. Fluid Mech. (1997), *vol.* 338, *pp.* 363–385

Shear-free turbulence near a wall

By DAG ARONSON[1], ARNE V. JOHANSSON[2] AND LENNART LÖFDAHL[1]

[1] Thermo and Fluid Dynamics, Chalmers University of Technology, S-41296 Göteborg, Sweden

[2] Royal Institute of Technology, Department of Mechanics, S-100 44 Stockholm, Sweden

(Received 20 June 1995 and in revised form 20 November 1996)

The mean shear has a major influence on near-wall turbulence but there are also other important physical processes at work in the turbulence/wall interaction. In order to isolate these, a shear-free boundary layer was studied experimentally. The desired flow conditions were realized by generating decaying grid turbulence with a uniform mean velocity and passing it over a wall moving with the stream speed. It is shown that the initial response of the turbulence field can be well described by the theory of Hunt & Graham (1978). Later, where this theory ceases to give an accurate description, terms of the Reynolds stress transport (RST) equations were measured or estimated by balancing the equations. An important finding is that two different length scales are associated with the near-wall damping of the Reynolds stresses. The wall-normal velocity component is damped over a region extending roughly one macroscale out from the wall. The pressure–strain redistribution that normally would result from the Reynolds stress anisotropy in this region was found to be completely inhibited by the near-wall influence. In a thin region close to the wall the pressure–reflection effects were found to give a pressure–strain that has an effect opposite to the normally expected isotropization. This behaviour is not captured by current models.

1. Introduction

In the computation of turbulent flows with engineering turbulence models there are a number of factors that determine the accuracy of the predictions. The numerical aspects are many and complex, e.g. choice of numerical solution algorithms and grid independence checks. Single-point closures of turbulence are often developed by validation against homogeneous turbulent flows. This is, to some extent, a reasonable approach and gives at least a platform to work from. One of the major obstacles though in obtaining an increased generality of the models is the treatment of near-wall effects and the choice of wall boundary conditions. Various types of wall-damping functions for different terms and 'low Reynolds number formulations' of the equations have been proposed. Modern advanced models that ensure realizability in the two-component limit constitute approaches that reduce the need for wall-damping functions at least to some extent. The two-component limit is approached near a solid wall, where the wall-normal component of the Reynolds stress vanishes more rapidly than the tangential ones. The presence of the wall is felt in several ways. The no-slip condition together with the mixing effect of the turbulence gives a thin region of strong mean shear in the boundary layer. Also, appreciable second-order derivatives of the mean velocity profile are restricted to a thin region close to the wall.

Regardless of the mean shear, the wall has a strong influence on the flow field. In the present paper we will investigate the wall influence on the turbulence field in the vicinity of a solid wall in the absence of mean shear. In this situation we have the influence of wall pressure reflection effects and viscous damping of the velocity fluctuations due to the no-slip condition.

When a solid wall is suddenly introduced into an initially isotropic turbulence field, or when isotropic turbulence passes with a uniform mean velocity over a solid wall that moves with the same velocity, multiple effects are introduced. Inhomogeneity in the turbulence statistics in the wall-normal direction is produced, while the isotropy in the wall-parallel plane is retained.

The first experimental study of this flow situation was carried out by Uzkan & Reynolds (1967), who conducted an experiment in a water tunnel for a mesh-size Reynolds number of $Re_M = 5000$ (turbulence Reynolds number $Re_T \equiv k^2/\nu\varepsilon \approx 90$). Distributions of the streamwise turbulence intensity were determined at a number of streamwise locations. These were found to collapse when normalizing the distance from the wall with a viscous length scale. Thomas & Hancock (1977) conducted a similar experiment in a wind tunnel at a much higher Reynolds number, $Re_M = 10^5$ ($Re_T \approx 2000$). These measurements were more detailed and included all the turbulence intensities. It is generally agreed that the main effect of the wall is the production of a 'splashing effect' near the wall, dominated by a transfer of energy from the wall-normal component to the wall-parallel ones. The results of Thomas & Hancock show, in contrast to the Uzkan & Reynolds results, but perhaps in intuitive agreement with the above notion, a distribution of the streamwise turbulence intensity with a peak substantially higher than the free-stream value. However, it is noteworthy in the Thomas & Hancock measurements that the spanwise intensity did not exhibit the peak found in the streamwise component. Hunt & Graham (1978) addressed these wall effects theoretically and attempted to reconcile the differences between the two aforementioned measurements. Brumley (1984) reviewed experiments on turbulence generated by e.g. an oscillating grid near a shear-free boundary. This case has definite similarities with the one considered here, although in the former the boundary is a fluid–air interface, which can be regarded as an inviscid boundary, in contrast to a solid wall. The lack of viscous damping of the velocity fluctuations lends a distinctly different character to the flow near an inviscid boundary.

An early numerical simulation of turbulence above a solid wall without mean shear was carried out by Biringen & Reynolds (1981) who used a large-eddy simulation method. Although these calculations were quite limited by grid resolution, the results agreed qualitatively with those of Uzkan & Reynolds (1967). Recently Perot & Moin (1995) reported an extensive DNS study of shear-free turbulent boundary layers. The influence of a wall was analysed by considering various fundamental types of boundaries, such as an idealized permeable wall, an idealized free surface and a solid wall, thereby isolating viscous and inviscid mechanisms. The relative importance of dissipation, inter-component energy transfer and energy transport was indicated from distributions of Reynolds stresses and the budget of the Reynolds stress transport (RST) equations. They also tried to relate the variation of the inter-component transfer to changes in the character of the turbulence structures as the wall is approached. Perot & Moin (1995) found no persisting near-wall peak in the streamwise Reynolds stress, i.e. contrary to the findings of Thomas & Hancock (1977). The work by Uzkan & Reynolds (1967), Thomas & Hancock (1977), Hunt & Graham (1978) and Perot & Moin (1995) has shown that the physical effects of a wall on the turbulence field are extremely com-

plicated even in the absence of mean shear. A scenario has been suggested whereby wall blocking effects amplify tangential intensities while viscous effects damp them. In homogeneous flows the energy transfer is commonly associated with the pressure–strain rate term, although also anisotropic dissipation can play a significant role. For inhomogeneous flows diffusion may also have a profound influence on the energy redistribution.

The present results demonstrate that in a thin region near the wall the pressure–strain has an effect opposite to that of the normally expected isotropization. Here, due to the presence of the wall, it transfers energy from the 'poor' wall-normal component to the 'rich' lateral ones. The results also show, in agreement with the DNS results of Perot & Moin (1995) and in contrast to the earlier experimental results of Thomas & Hancock (1977), that viscous diffusion and dissipation counteract the effects of energy transfer to the lateral components to a degree so as to give intensity distributions without significant near-wall peaks.

The objective of the present study is to improve the understanding of the physics involved in the interaction of turbulence with solid walls. This is accomplished with an experimental investigation of decaying grid-generated turbulence passing over a flat solid surface moving with the mean velocity of the fluid. Effects of mean shear are thereby excluded. Particular attention has been paid to the construction of the experimental facility in order to minimize the mean velocity gradient and to ensure a good uniformity of the turbulence statistics. Hot-wire anemometry is used to determine quantities of interest for modelling the RST equations and their near-wall behaviour. Existing models of wall-reflection terms for the pressure–strain rate and the treatment of the near-wall behaviour of the diffusion and dissipation terms are discussed.

2. Experimental apparatus and procedure

The experimental realization of decaying turbulence near a solid boundary without mean flow inhomogeneities is accomplished by passing grid-generated turbulence over a wall moving with the stream speed (see 1 in figure 1). The wind tunnel used is a low-speed closed-circuit tunnel with a test section of $1.25 \times 1.80 \times 2.90$ m^3 and a contraction ratio of 6.2. The tunnel is equipped with a cooling system capable of keeping the temperature variations of the moving fluid to less than 1°C during the measurements. The free-stream velocity, U_∞, and hence the moving wall velocity, were 5 m s^{-1} in all experiments reported here.

A major difficulty in this experimental realization is to introduce the moving wall without creating significant disturbances. Typical sources of disturbances are the influences of wind-tunnel wall boundary layers, the effects of incorrectly balanced velocity distributions of the suction channels used to remove the wind-tunnel wall boundary layer, and 'buoyancy' effects caused by frictional heating at the boundary between the moving belt and the backing plate. In a shear-free boundary layer such disturbances can be particularly severe since the mean shear and the associated turbulence production, which otherwise quickly would reorganize the turbulence, are absent and any initial disturbance would propagate a long distance downstream.

2.1. *Moving wall*

The floor of the working section was replaced by an endless belt mechanism in order to match the wall and the free-stream velocities. Figure 1 shows a sketch of the complete moving belt arrangements. The belt dimension was $0.002 \times 0.98 \times 4.17$ m^3

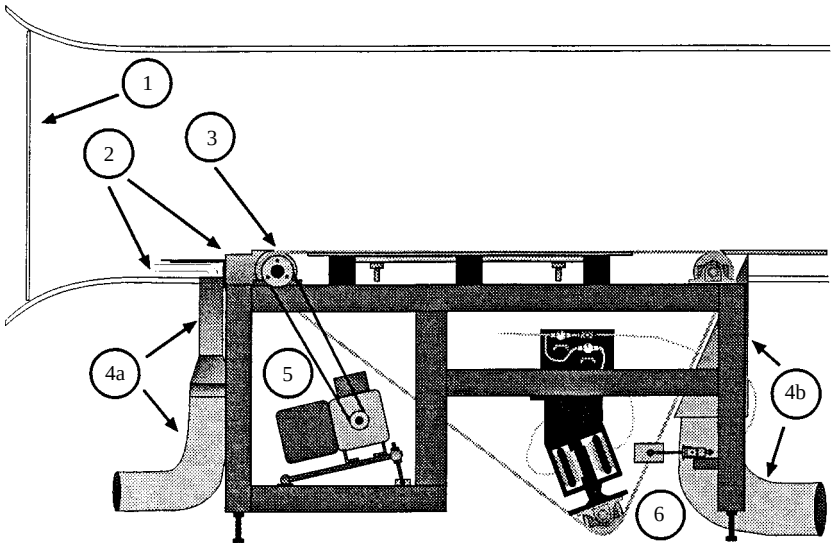

FIGURE 1. Schematic diagram of the wind tunnel, turbulence generation grid and moving wall arrangement. Grid mesh width is 80 mm and distance between moving and top walls is 1.08 m. Length of the moving wall section is 1.7 m. 1–6 are described in the text.

and covered the full width of the working section. In the present experiments the length of this section corresponds to approximately one and a half eddy turnover distances $\left(U_\infty k_o/\varepsilon_o\right)$, where k_o and ε_o are the turbulent kinetic energy and dissipation rate at the beginning of the moving wall. As shown in the figure, the belt runs over three circular cylinders of 150 mm diameter, and a pneumatic device (6 in figure 1) was used to control and adjust the lateral position of the belt. Any movement sideways was detected by a sensor, and a deviation from the nominal value was immediately counteracted by displacing one of the two end supports of the lower cylinder. When performing hot-wire measurements close to a surface, no vertical motion or vibrations of the belt can be accepted. These were eliminated by a smooth backing-plate in combination with a high tension of the belt. To prevent any buoyancy effects caused by frictional heating at the boundary between the belt and the backing-plate, the latter was water cooled. Tests showed that a temperature variation of less than $\pm 0.5^\circ$C was obtained during the measurements. The belt was driven by an electrical motor (5 in figure 1), which was connected to a frequency converter so the rotational speed could be adjusted continuously between zero and the maximum speed. During all measurements the speed of the belt was checked by focusing a stroboscope on a scale on the belt.

A major difficulty in forming a shear-free boundary layer is the elimination of the wall boundary layer formed in the contraction part of the wind tunnel. One method typically used is to employ suction through a porous wall. An alternative approach is to remove the tunnel boundary layer through a duct with suction, i.e. 'shave off' the boundary layer by a reduction of the tunnel cross-section. The latter method was used in this work. To make the wall boundary layer removal smooth, the reduction of the tunnel cross-section was made in two steps and the oncoming flow towards the moving belt was controlled by a leading edge (2 in figure 1). Here, the length of this leading edge was determined as a compromise between the desire to minimize the upstream disturbances on the belt (i.e. a short leading edge) and the need for

an appropriate curvature around the upstream roller (i.e. a certain minimum length). Moreover, to prevent fluid from being advected by the belt over the first roller into the tunnel, the size of the gap between the suction box and the first roller (3) was minimized and a small suction applied. The flow balance of the wind tunnel was maintained by recirculating (4a, 4b in figure 1) all of the evacuated air into the tunnel as shown in figure 1.

2.2. *Measurement procedure*

The turbulence measurements were made using a constant-temperature anemometer and standard Dantec miniature hot wires, single as well as cross wires, made of tungsten and with an active length of 1.25 mm and a diameter of 5 μm. A computerized traversing mechanism attached to the upper wall of the wind tunnel allowed the probes to be moved in the streamwise and normal directions. For all the data acquisition a Macintosh-based computer system was used. A look-up table was used to relate voltages to velocities for the X-wire probes, see Lueptow, Breuer & Haritonidis (1988), and the single wires were calibrated directly using the transfer function suggested by Collis & Williams (1959).

A key feature of this experiment was the ability to measure accurately and with good resolution the fluctuating velocity gradients forming the dissipation rate tensor. For a proper determination of these gradients it is important to assess the spatial filtering arising from the finite length of the wires and from the finite separation of multiple wires. For velocity measurements, these effects have been analysed by Wyngaard (1968), Ligrani & Bradshaw (1987) and Browne, Antonia & Shah (1988). Wyngaard (1968) made a theoretical study of how finite wire length influences the measured spectra, and concluded that the spatial dimensions of the probe should be of the order of the Kolmogorov microscale, $\eta = \left(\nu^3/\varepsilon\right)^{1/4}$, to minimize the effects of spatial filtering. Wires of large L/η, where L is the length of the hot wire, give errors due to their lack of spatial resolution of the fine scales of the flow resulting in an attenuation of the high frequencies. From an experimental investigation Ligrani & Bradshaw (1987) found an optimal sensor performance is obtained using $L/\eta = 1.6$ and $L/d = 260$. Wires of small L/d give errors due to end conduction effects, resulting in an attenuation of the measured intensities. Browne *et al.* (1988) studied the influence of wire spacing of X-probes in obtaining $\overline{u_1^2}$, $\overline{u_2^2}$ and $\overline{u_1 u_2}$. Their experiments were conducted in the far wake of a circular cylinder. In order to limit the error due to wire spacing to no more than 4% as compared to the value measured by a single hot wire, they found that the wire spacing not should exceed approximately 3η, provided $L/d = 150$ and $L/\eta = 1.7$.

The effects of wire spacing, i.e. spatial filtering, on the measurements of the variance of $\partial u_1/\partial x_2$ have been analysed by e.g. Wyngaard (1969), Ewing & George (1994) and Antonia & Mi (1993). These papers suggested a separation between the hot wires in the range of 2η–4η.

Figure 2 shows the measured value of the velocity derivative moments $\overline{\left(\partial u_1/\partial x_i\right)^2}$, approximated by $\overline{\left(\Delta u_1/\Delta x_i\right)^2}$, as a function of wire separation. Theoretically, this estimate becomes more accurate as $\Delta x_i \to 0$, but as the wire separation decreases, the relative error of Δx_i increases, and errors associated with the resolution of the A/D-converter and noise contamination from the anemometer and other parts of the electronic system will also become significant, giving a systematic increase of $\overline{\left(\partial u_1/\partial x_i\right)^2}$ as the wire separation decreases (figure 2). Also noteworthy is that this

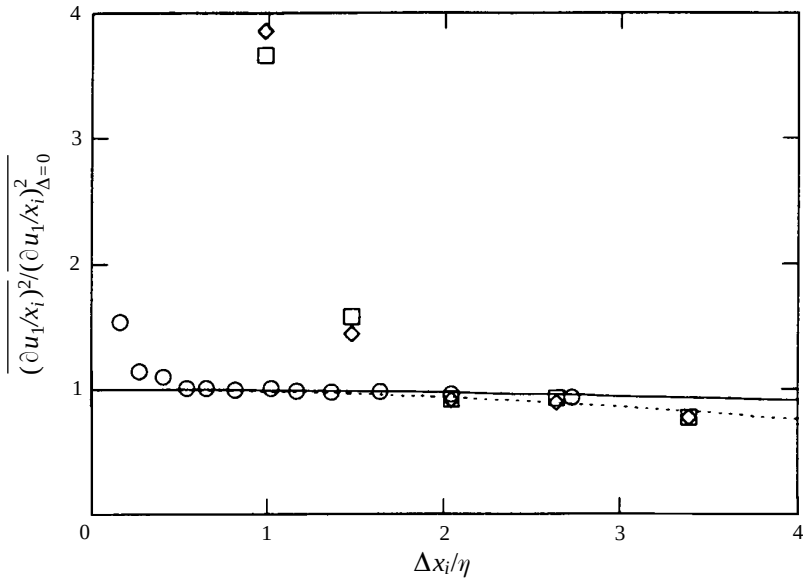

FIGURE 2. Effect of wire spacing on the measurement of the variance of $\partial u_1/\partial x_i$. ○, $i = 1$; □, $i = 2$; ◇, $i = 3$.

effect is more accentuated for measurements of the cross-stream derivative moments. On the other hand, if the separation between the wires is too large, the small scales will not be resolved yielding too small a value of $\overline{(\partial u_1/\partial x_i)^2}$. As pointed out by several investigators, the measured velocity derivative variance closely adheres to the following expression in an intermediate region:

$$\overline{\left(\frac{\partial u_1}{\partial x_i}\right)^2}_M = \overline{\left(\frac{\partial u_1}{\partial x_i}\right)^2}\left(1 + C\left(\frac{\Delta x_i}{\lambda}\right)^2\right) \tag{2.1}$$

where λ is an appropriate Taylor microscale and C is a constant expected to be of order unity.

Using this relation we can obtain the desired velocity derivatives from an extrapolation of measurements within this region. For the cross-stream derivatives wire separations $\Delta x_i/\eta$ of 2.0 and 2.6 were used, and the length of the wires was 1.8η.

Other possible sources of error in derivative measurements are the drift in the calibration of one wire relative to the other and the temperature–wake interaction. To determine the former we repeatedly returned to a reference position during the series of measurements in order to determine the same derivatives. No significant deviations were noted. The wake interaction is more accentuated for cross- than for parallel-wires, and since comparatively large probes were used this source of error was judged to be negligible.

3. The grid-generated turbulence

The homogeneous isotropic flow field was generated by passing the undisturbed flow through a grid. The choice of dimensions for the grid is governed by a number of different (and partially opposing) criteria (various experimental aspects of turbulence-generating grids are discussed by e.g. Corrsin 1963). A small mesh width is desirable

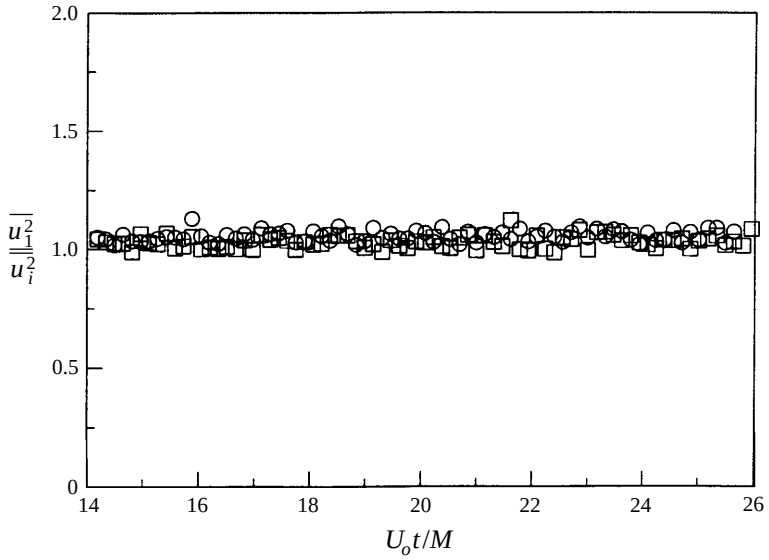

FIGURE 3. Downstream distribution of anisotropy with the grid located in the contraction part of the wind tunnel. ○, $i = 2$; □, $i = 3$.

from the view point of obtaining a large number of eddy turnover times during the passage of the turbulence over the moving wall. For homogeneity reasons the ratio of the mesh width to wind tunnel height should at least be smaller than 0.1 (see Roach 1987), and spatial resolution requirements call for a large mesh size in order to fulfil the above discussed requirements for the ratio of hot-wire length to Kolmogorov scale.

For the present purposes it is important that the grid is a monoplane one since otherwise substantial anisotropies will occur, see Groth, Hallbäck & Johansson (1989). The grid was accurately manufactured from aluminium pipes of square cross-section (side 15 mm) to give a mesh size of 80($\pm$0.05) mm, and a solidity (projected solid to total area) of 0.34. Optimum experimental conditions with the moving belt described in §2.1 were obtained with a wall velocity of 5 m s^{-1} giving a mesh Reynolds number of about 1.6×10^4.

It was found in initial experiments that, with the grid positioned in the beginning of the test section, the ratio $\overline{u_1^2}/\overline{u_2^2}$ attains a value of about 1.2 at the position of the moving wall. This value is fully in accordance with what has been found in numerous investigations, see e.g. Comte-Bellot & Corrsin (1966). They made use of the well-known fact that a contraction reduces the relative streamwise intensity to a larger degree than the lateral ones and achieved a practically isotropic turbulence by use of a contraction with an area ratio of 1.3 some distance downstream of the grid. We here adopted a slightly different approach and positioned the grid in the contraction part of the wind tunnel. This technique is well established, and has been tested and shown to give good homogeneity of the turbulence both in connection with the present experiments and with experiments by e.g. Sjögren & Johansson (1996). The present technique requires a somewhat larger contraction ratio to achieve isotropy and in the experiments the area ratio for the part downstream of the grid was chosen as 1.6, which resulted in a very low degree of anisotropy, $\overline{u_1^2}/\overline{u_2^2} \approx 1.02$, as is shown in figure 3. The difference, compared to the value used by Comte-Bellot & Corrsin (1966),

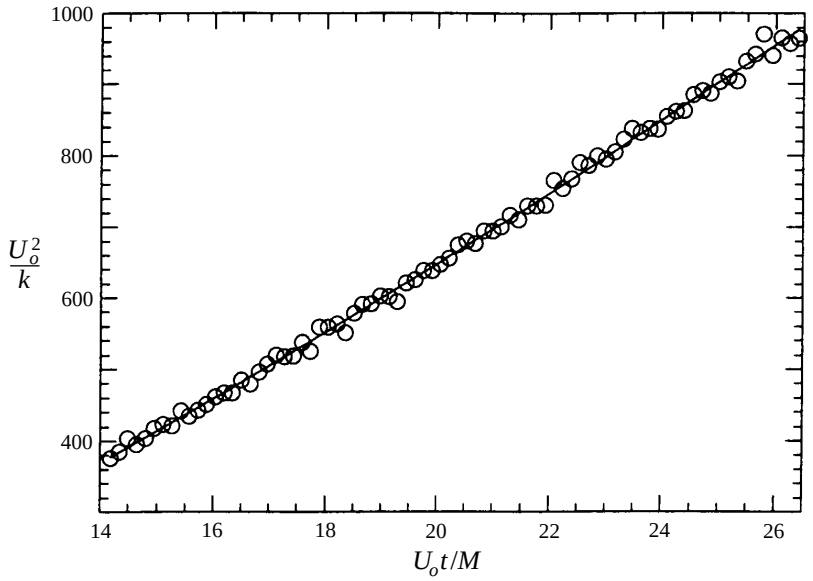

FIGURE 4. Downstream decay of kinetic energy The leading edge of the moving belt arrangement is located at $U_0 t/M = 14.3$.

is related to the fact that the grid here is placed in the contraction and the strain thereby acts during the generation process.

The error of $\overline{u_1^2}$ was found to be less than 1%. This value is based on repeated measurements with different hot-wire probes. Using this approach the uncertainty of $\overline{u_2^2}$ and $\overline{u_3^2}$ was found to be less than 2–3%.

The present experimental set-up was used with $U_\infty = 5$ m s^{-1} in the following experiments, and resulted in an integral scale, $L_{int} \approx 31$ mm, and a Kolmogorov microscale, $\eta \approx 0.6$ mm, at the measuring position (η is obtained in the free stream using the isotropic expression for ϵ. Hence, with a wire length of 1.08 mm ($L/d = 216$) we have fulfilled the requirements discussed in §2.2.

In assessing the performance of the grid, it is customary to fit the grid turbulence decay data with power laws over various periods of decay of the turbulence. Therefore, following the example of Batchelor & Townsend (1948), we fit power laws for $1/k$, where k is the turbulent kinetic energy, $k \equiv \overline{u_i u_i}/2$, and L_{int}. Since the actual grid location is irrelevant in the fully developed range, we use the empirical forms:

$$\frac{U_o^2}{k} = A_1 \left(\frac{U_o t}{M} - \frac{U_o t^*}{M} \right)^{n_1}, \tag{3.1}$$

$$L_{int} = A_2 \left(U_o t - U_o t^* \right)^{n_2}, \tag{3.2}$$

where $L_{int} = \int_0^\infty \overline{u_1(0) u_1(x_1)} \mathrm{d}x_1 / \overline{u_1^2}$.

Figure 4 shows a typical decay of turbulent kinetic energy as a function of $U_o t/M$, where U_0 is the mean speed at the grid and t is the elapsed time calculated from $t = \int \mathrm{d}x/U_1(x_1)$. The coefficients of (3.1) were determined by least-square fit to the experimental data, and a comparison with the corresponding measurements of Comte-Bellot & Corrsin (1966) is shown in table 1. As is evident from the table the two experiments display very similar decay rates. The downstream development of the 'longitudinal' integral scale is shown in figure 5. A best fit to the data is made after

Reference	$U_o t^*/M$	k-decay n_1	A_1
Present	3.2	1.27	18
		$\overline{u_1^2}$-decay	
Comte-Bellot & Corrsin (1966)	3	1.29	19
Present	3.2	1.26	27

TABLE 1. A comparison of the present energy decay rate of the grid turbulence to corresponding data of Comte-Bellot & Corrsin (1966).

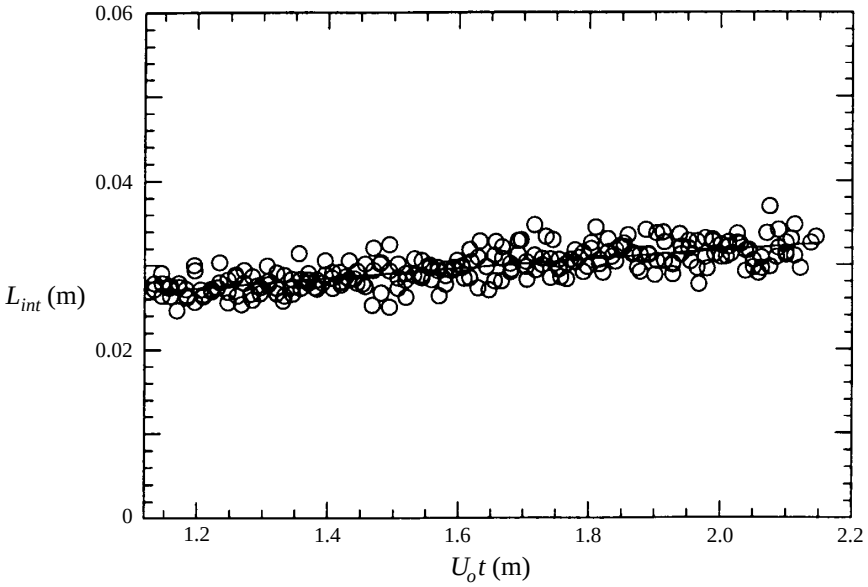

FIGURE 5. Downstream development of the integral scale.

prescribing a value of 0.50 for the exponent in (3.2) (see p. 73 in Tennekes & Lumley 1972). A lower value, $n_2 = 0.35$, was found by Comte-Bellot & Corrsin (1966). The fit seen in figure 5 is actually quite insensitive to the specific choice of the exponent.

As is evident from figure 3, the degree of Reynolds stress anisotropy is low. However, since this measure is dominated by the large scales of the turbulence, it may only be interpreted as an indication of the isotropy of the turbulence. A measure of the degree of isotropy in the small scales is the ratio of the different components forming ε. In figure 6, the ratio $2\overline{(\partial u_1/\partial x_1)^2}/\overline{(\partial u_1/\partial x_2)^2}$, which for an isotropic flow field should equal unity, is shown as a function of the distance from the wall. Close to the wall there is a strong degree of anisotropy due to the action of the fluctuating viscous shear near the wall. As is obvious from the no-slip condition, the numerator of the above expression must approach zero at the wall while the denominator remains finite. Hence, the ratio must tend to zero near the wall. As the distance from the wall increases it approaches unity, indicating a shift towards isotropy in the small scales of the free stream. This also indicates that the isotropic estimate of the dissipation rate in the free stream should be approximately correct.

The value of the dissipation rate, ε, obtained as $-U_1 \partial k/\partial x_1$ from the kinetic energy

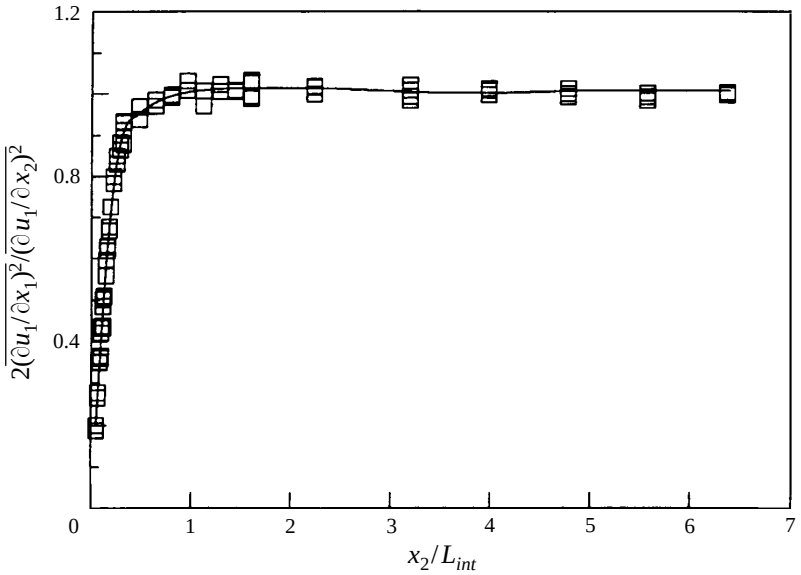

FIGURE 6. Distribution of the measure of isotropy as a function of the distance from the wall, at the measuring position $x/M = 16.2$.

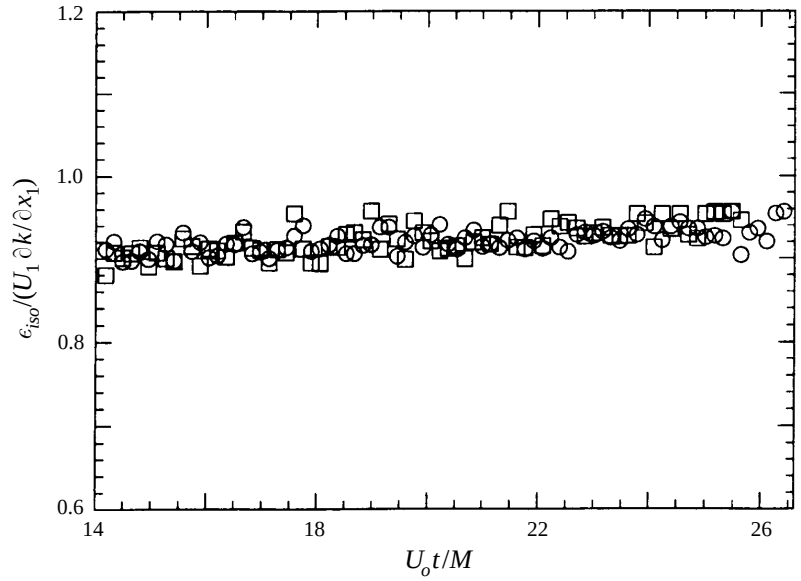

FIGURE 7. Downstream development of the ratio between the isotropic estimate of the dissipation rate and that obtained from the kinetic energy budget.

budget, can be compared with the isotropic estimate, $\varepsilon_{iso} = 15\nu\left(\overline{\partial u_1/\partial x_1}\right)^2$, see e.g. Tennekes & Lumley (1972). Figure 7 shows that the ratio of the isotropic estimate of the dissipation and the value determined from the energy budget increases from approximately 0.9 at the beginning of the test section towards unity as the downstream distance increases. This indicates an approach towards an isotropic state. Also the resolution of the small scales becomes slightly better with increasing downstream

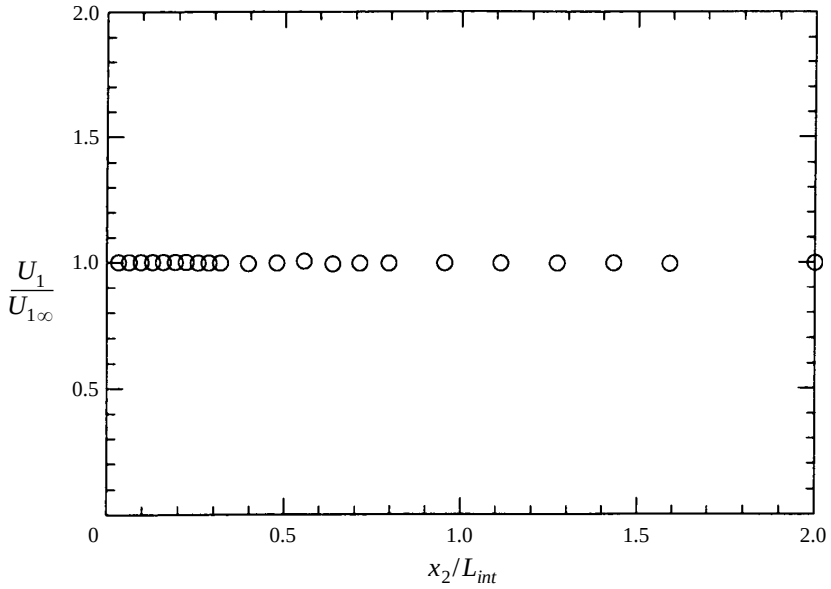

FIGURE 8. Mean velocity distribution at the measuring location $x/M = 16.2$.

distance (see Ewing & George 1994). Moreover, the diffusion is not accounted for in this estimate, but should have a quite small influence here. For the present purposes we may conclude that it is possible to obtain a reasonable resolution of the small scales using the current measuring technique, and that the anisotropy in the free stream seems to be low in the large as well as in the small scales.

4. Results and discussion

All measurements presented here were conducted at a mesh Reynolds number, $Re_M = 1.6 \times 10^4$ ($U_\infty = 5\text{m s}^{-1}$). The turbulence Reynolds number, $Re_T(k^2/v\varepsilon)$, varies from approximately 325 to 425 through the measuring section. All distances along the moving belt are measured from the leading edge and scaled with the mesh width. At the measuring position, $x/M = 16.2$, the turbulence Reynolds number is roughly the same as the largest value studied by Perot & Moin (1995).

We will in the following discuss flow phenomena associated with the introduction of a rigid surface into a homogeneous turbulent field, the flow development along the moving belt and the turbulence field at the measuring position. Moreover, the terms of the streamwise Reynolds stress transport equation are estimated, and a comparison is made between the balanced streamwise pressure–strain rate term and some current model predictions of this term.

4.1. *Mean velocity and turbulence statistics*

A flow without any mean flow inhomogeneities was accomplished as described in §2.2, and a typical mean velocity profile at the measuring position is shown in figure 8. Throughout the region of interest, the variation was less than 1.0%. This was considered to be satisfactory and hence, in the absence of a mean velocity gradient, the production of turbulence was negligible along the moving belt.

The sudden change of boundary condition has an immediate effect on the turbulence field. The data shown in figure 9, which were taken one integral scale downstream of

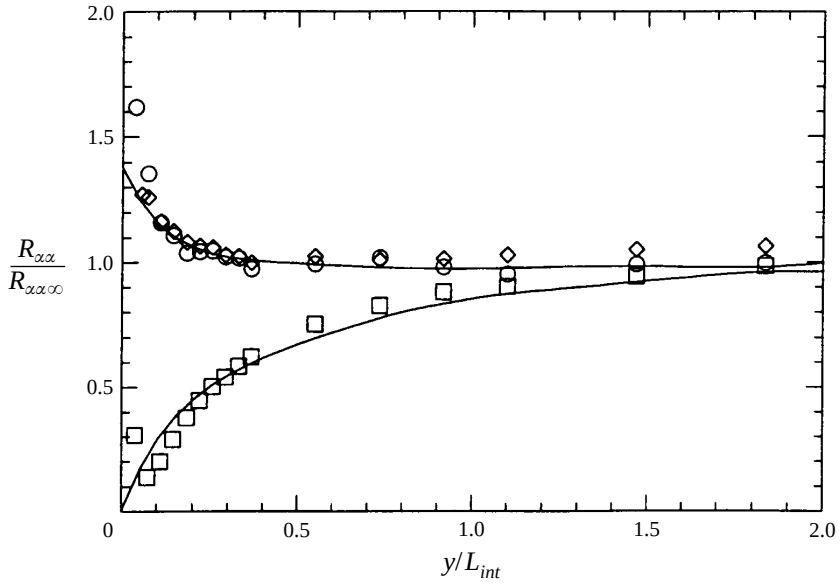

FIGURE 9. Reynolds stress vs. wall distance at one integral scale downstream of the leading edge. ○, $\alpha = 1$; □, $\alpha = 2$; ◇, $\alpha = 3$ (no summation over Greek indices). The solid lines are the predictions of the Hunt & Graham theory.

the leading edge, show substantial influence on the intensities up to wall distances of the order of one integral scale.

The problem of suddenly inserting a rigid boundary, moving with the stream speed, in a turbulent flow field has been studied theoretically by Hunt & Graham (1978), who proposed a method of accounting for the effects on the turbulence field. The analysis is based on the linearized equations for the fluctuating velocity and vorticity, so that a low level of turbulence intensity is assumed. Hunt & Graham (1978) describe the effects of the wall on the flow field in terms of two distinctly different layers: a viscously dominated region close to the wall and an inviscid region further out. The neglect of viscous influence in the outer region will, however, be less accurate as the distance travelled downstream increases because of accumulated effects of the viscous stresses. One should keep in mind that there is no regeneration of turbulence in this case. In the viscously dominated near-wall region the pressure terms were assumed to be negligible.

The resulting equations were subsequently solved in spectral space, and the results express the final spectra in terms of initial ones. Mean-square values of the fluctuating components, $\overline{u_i^2}$, were calculated for two different initial spectra and the result for the outer inviscid region shows that energy is transferred from the normal to the tangential components, which show an increase as the wall is approached. A solution for the near-wall region was also put forward by Hunt & Graham (1978). Since the equations in this region have the typical form of a heat or diffusion equation an error function will describe the velocity distributions, and the thickness of this layer will be proportional to $(\nu t)^{1/2}$. Moreover, in Hunt & Graham it is also stated that the theory is applicable to the flow near a semi-infinite flat plate provided the displacement thickness of the boundary layer on the plate is sufficiently thin.

In our experiment, the assumptions used by Hunt & Graham (1978) are fulfilled in the region near the leading edge. A comparison of the present measurements

with the theory is shown in figure 9 at a downstream distance of one integral scale. Note that the two tangential components display the same behaviour, within the experimental error, as was expected since the flow field should be axisymmetric, i.e. isotropic in planes parallel to the wall. Another important feature is that after this short downstream distance, the normal component of the Reynolds stress has already been damped over a comparatively large normal distance, about one to two integral scales, while the tangential components are affected only over less than half an integral scale out from the wall. At this small distance from the leading edge, the analysis of Hunt & Graham (1978) captures the essential behaviour of the flow. However, further downstream the neglected terms of the governing equations become of increasing importance. This implies that the influence of the viscosity must be considered and one should expect an attenuation of the near-wall peak in the tangential components.

The downstream development of the streamwise, $R_{11}/R_{11\infty}$, and normal $R_{22}/R_{22\infty}$, Reynolds stresses is shown in figures 10(*a*) and 10(*b*), respectively. The solid lines represent best-fit distributions at the respective positions. As is evident from the figures, the distribution of the streamwise Reynolds stress goes through a dramatic change, while the normal component is almost unaffected. Here, the wall distance is normalized by the integral scale in the free stream. As would be expected from the theory of Hunt & Graham the collapse of the curves for the streamwise Reynolds stress for different x/M is significantly better in the near-wall region, although still far from perfect, when the wall distance is normalized by $(vt)^{1/2}$.

The initial near-wall peak in the streamwise Reynolds stress is caused by energy transfer from the normal component into the tangential ones as an adjustment to the rapid change in the boundary conditions as the turbulence passes over the solid surface (cf. the Hunt & Graham theory). This peak, which is also found in the spanwise Reynolds stress (see figure 9), rapidly decreases and has practically vanished at the measuring position of $x/M = 16.2$ (corresponding to approximately 1.1 eddy-turnover times). Noteworthy is also that the streamwise component is affected only close to the wall, $x_2/L_{int} \approx 0.2$–0.3, while the normal component is influenced over a much larger distance, of the order of 1–2 integral scales, from the wall. The latter has essentially already been established in the initial adjustment to the new boundary conditions.

Hence, we can identify two regimes in the development of the shear-free boundary layer. The first region may be characterized as an adjustment regime of one to two eddy-turnover times where the near-wall peak in the tangential components 'rapidly' decreases. The presence of the wall causes a shear in the tangential components of the fluctuating velocity field and thus gives an enhanced viscous influence on these components, which significantly contributes to the relaxation of the near-wall peak. In the second regime the Reynolds stresses vary quite slowly with downstream distance, and this can be at least partly understood from the fact that the intensities and integral scale in the free stream exhibit only a slow variation with downstream distance.

The observations are in agreement with the DNS results of Perot & Moin (1995), who were able to study the turbulence at different Reynolds numbers for as long as three eddy turnover times. Their temporally growing shear-free boundary layer can be approximately related to the spatially growing shear-free boundary layer studied here through the use of Taylor's hypothesis. The position $x/M = 16.2$ translates to $t/T = 16.2\left(M/U_\infty\right) / \left(L_{int}/(2k/3)^{1/2}\right) \approx 1.1$. In the simulations of Perot & Moin (1995) a near-wall peak in the tangential Reynolds stresses was caused

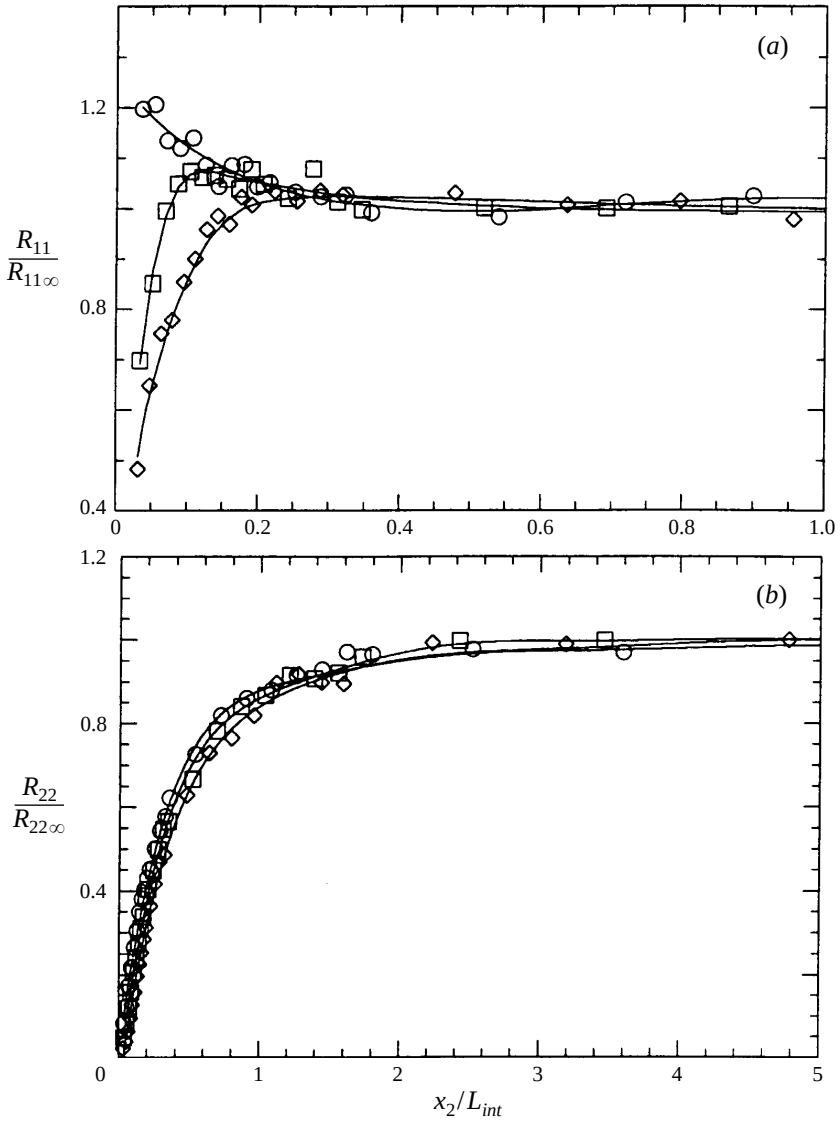

FIGURE 10. Downstream development of (*a*) the streamwise Reynolds stress and (*b*) the normal Reynolds stress. ○, $x/M = 3.5$; □, $x/M = 7.4$; ◇, $x/M = 16.2$. Solid curves represent the best fit to the respective data set.

by the suddenly imposed boundary condition on the initially isotropic turbulence. For their largest Reynolds number it had practically vanished after roughly one to two eddy turnover times, which is in accordance with the findings in figure 10(*a*). It is noteworthy that this experiment, the DNS of Perot & Moin (1995) and the work of Uzkan & Reynolds (1967) do not indicate any near-wall peak after a sufficient downstream distance/time. This is contradictory to the results of Thomas & Hancock (1977), who found a persisting increase of the streamwise Reynolds stress as the wall was approached. Moreover, they found that the peak grew significantly with downstream distance.

The present results for the individual Reynolds stresses are compared in figure

11(*a–c*) with the numerical results of Perot & Moin and the experimental results of Thomas & Hancock at a downstream position corresponding to roughly one eddy-turnover time. In this figure the symbols are used only to designate the different data sets (and do not mark individual measurement points). In general there is quite good agreement with the results of Perot & Moin whereas the data of Thomas & Hancock show a considerable discrepancy for the R_{11} component. It is noteworthy that their results for the R_{33} component exhibit only a weak near-wall peak that also decreases in magnitude with downstream distance, in accordance with the present results.

Possible influences of differences in Reynolds number have already been discussed by Hunt & Graham (1978), but this cannot be considered to be a plausible cause for the discrepancies between the Thomas & Hancock data and the present as well as the DNS results. Perot & Moin (1995) suggest that the measured streamwise tangential Reynolds stresses could have been contaminated by mean shear, despite the fact that considerable efforts were made to try to eliminate the mean shear. However, a more likely candidate for causing the near-wall peak in the streamwise Reynolds stress may be the effects of frictional heating between the belt and the backing plate. In the Thomas & Hancock experiments a temperature rise of 8°C at the boundary was noted during the measurements, while in our experiment the backing plate was water cooled, with a maximum temperature variation of less than 1°C. For hot-wire measurements in this geometry the influence of frictional heating on the determination on the different tangential turbulence intensities may be considerable. In order to check this effect, we increased the temperature of our backing plate to about 10°C above the wind-tunnel temperature. Repeated experiments showed that this temperature increase resulted in a significant increase of the streamwise Reynolds stress component as is shown in figure 12 and may be explained in the following way. The square of the output voltage, E, from the hot wire is proportional to the temperature difference between the wire and the ambient air. Introduce $\theta = T - T_\infty$, where T is the temperature at the measuring position and T_∞ is the ambient temperature at which the probe was calibrated. Then let θ' denote the turbulent fluctuation of θ and Θ denote the time-averaged value, $\overline{\theta}$. A small change in the ambient temperature then gives rise to a relative voltage change $\Delta E/E = -\frac{1}{2}\theta/\Delta T_w$, where ΔT_w is the overheat of the wire. The form of King's law, in turn, yields that the measured streamwise velocity u_{1m} can be written as

$$u_{1m} = u_1 \left(1 - c\frac{\theta}{\Delta T_w}\right). \tag{4.1}$$

For high velocities, the constant c approaches the inverse of the exponent in King's law and is larger for lower velocities. One should expect values of c typically in the range 3–4. It is obvious that an error is introduced if the temperature of the fluid is different from T_∞, and this can readily be shown to affect the measurements of mean velocity and the turbulence component as follows (assuming that $\overline{u_1'\theta'} \approx 0$):

$$\frac{\overline{U_{1m}}}{\overline{U_1}} = 1 - c\frac{\Theta}{\Delta T_w}, \tag{4.2}$$

$$\frac{\overline{(u_{1m}')^2}}{\overline{(u_1')^2}} = 1 + c^2\frac{\overline{U_1}^2}{\overline{(u_1')^2}}\,\frac{\overline{(\theta')^2}}{\Delta T_w^2} - 2c\frac{\Theta}{\Delta T_w} \approx 1 + c^2\frac{\overline{U_1}^2}{\overline{(u_1')^2}}\,\frac{\overline{(\theta')^2}}{\Delta T_w^2}. \tag{4.3}$$

This effect will not significantly affect the measurement of the other components

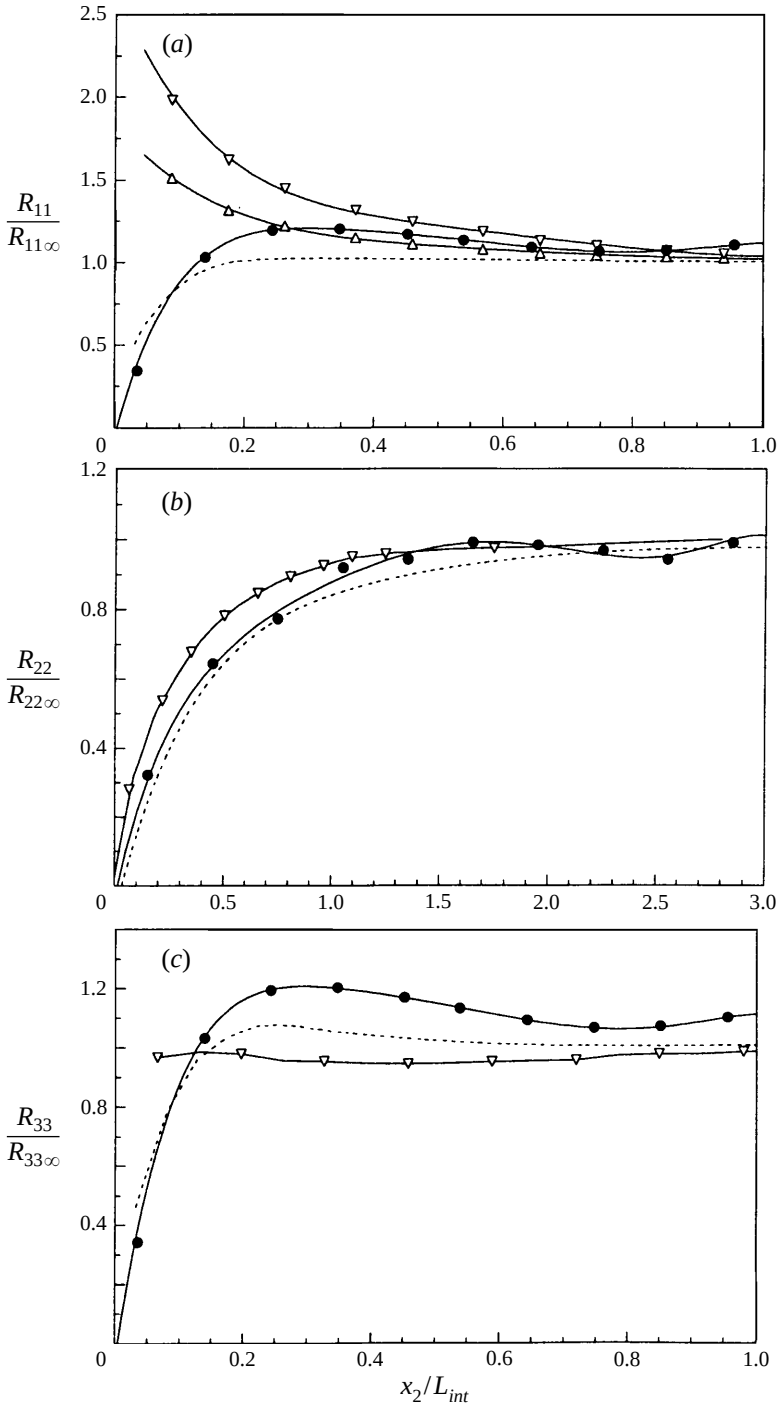

FIGURE 11. Comparison of (*a*) R_{11}, (*b*) R_{22} and (*c*) R_{33}. Dashed curve, present results at $x/M = 16.2$. Thomas & Hancock (1977): △, $x/M = 18.2$; ▽, $x/M = 21.4$. Perot & Moin (1995): •, $t/T = 1.1$. (All distances from the leading edge.)

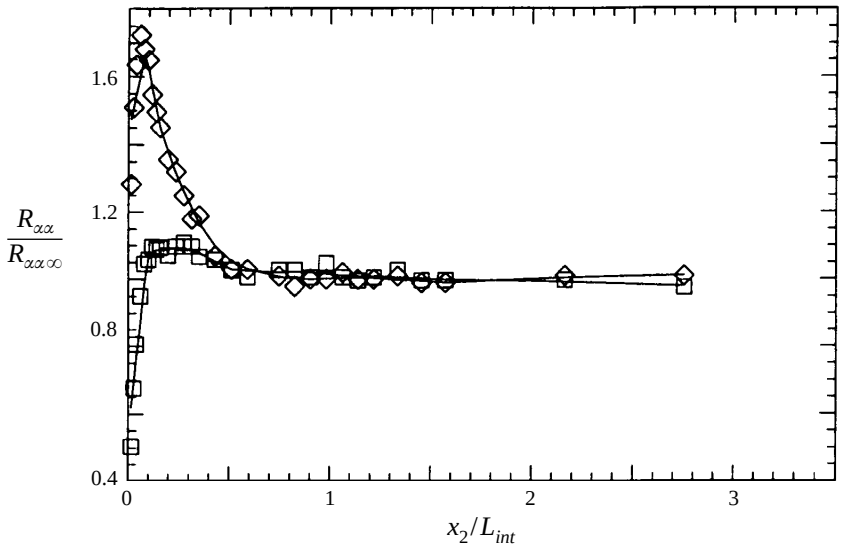

FIGURE 12. Distributions of Reynolds stresses vs. wall distance: ◇, $\alpha = 1$; □, $\alpha = 3$, wall heated above ambient temperature.

since it can easily be shown that

$$u_{2m} = u_2\left(1 - c\frac{\theta}{\Delta T_w}\right) = u_2'\left(1 - c\frac{\Theta + \theta'}{\Delta T_w}\right), \tag{4.4}$$

$$\frac{\overline{(u_{2m}')^2}}{\overline{(u_2')^2}} = 1 - 2c\frac{\Theta}{\Delta T_w}, \tag{4.5}$$

and similarly for the u_3-component. This implies that the effect is negligible for the normal and spanwise components and need only to be considered in the streamwise Reynolds stress. Also Smits & Perry (1981) show that the effect of an increase in temperature is negligible on the normal and spanwise turbulent components, whereas the effects on the streamwise component is significant. Hence, in the measurements of Thomas & Hancock (1977), see figure 11(*c*), the spanwise component displays a similar behaviour to our data, while there is a significant difference in the streamwise Reynolds stress component fully in accordance with the above analysis.

4.2. *Terms in the streamwise Reynolds stress transport (RST) equation*

The RST equations may be written in symbolic form as

$$\frac{\mathrm{D}R_{ij}}{\mathrm{D}t} = \mathscr{P}_{ij} - \varepsilon_{ij} + \Pi_{ij} + d_{ij}. \tag{4.6}$$

Here $R_{ij} \equiv \overline{u_i u_j}$; $\mathscr{P}_{ij} \equiv -\left(\overline{u_i u_k}U_{j,k} + \overline{u_j u_k}U_{j,k}\right)$ is the production rate tensor, the trace of which is responsible for the extraction of energy from the mean flow to the fluctuations, and here is zero; $\varepsilon_{ij} \equiv 2\nu\overline{u_{i,k}u_{j,k}}$ is the homogeneous dissipation rate tensor; $\Pi_{ij} \equiv \overline{(p/\rho)\left(u_{i,j} + u_{j,i}\right)}$ is the pressure–strain rate tensor; and $d_{ij} \equiv \left[\left(\overline{u_i p}\delta_{jk} + \overline{u_j p}\delta_{ik}\right)/\rho - \nu\left(\overline{u_i u_j}\right)_{,k} + \overline{u_i u_j u_k}\right]_{,k}$ is the transport or diffusion tensor. The latter term contains contributions from pressure diffusion, viscous and turbulent diffusion. Derivations of the RST equations can be found in most textbooks in the

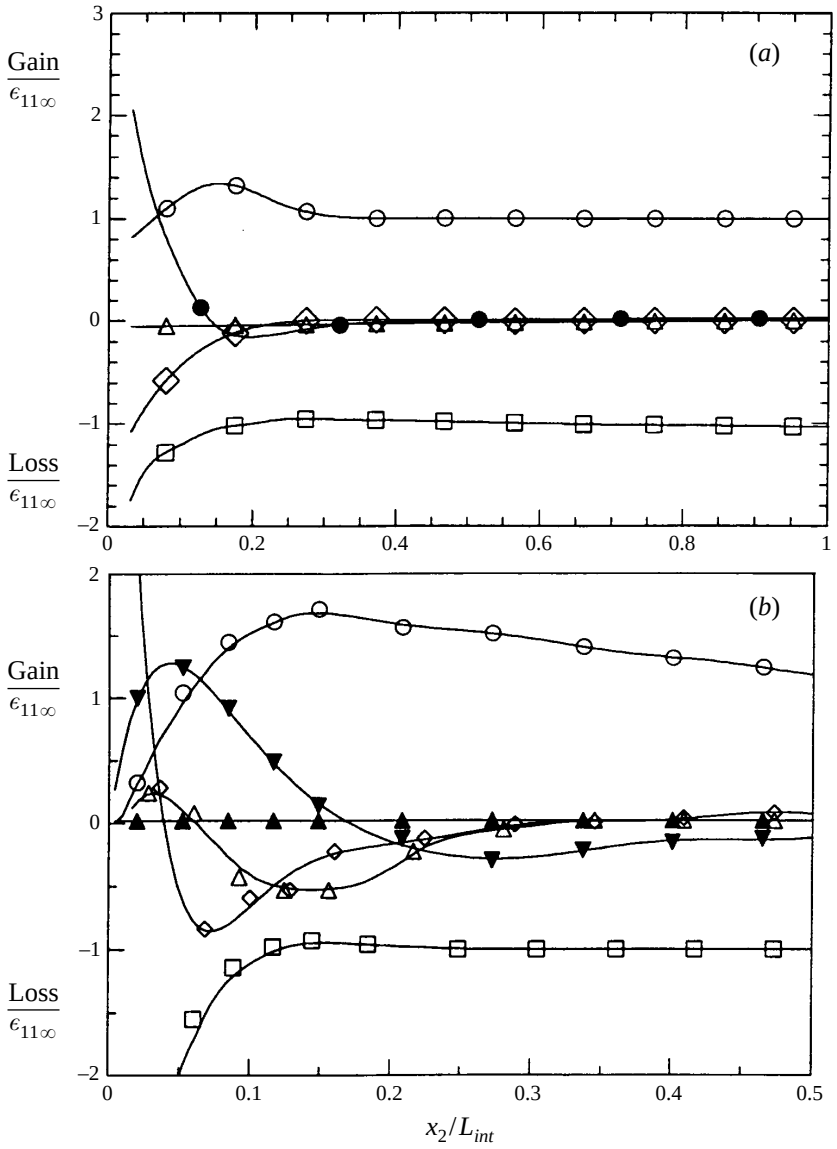

FIGURE 13. Terms in the streamwise RST equation as obtained from (*a*) the present experiments: ○, advection; □, dissipation; ◇, viscous diffusion; △, turbulent diffusion; •, pressure–strain and pressure diffusion and (*b*) Perot & Moin (1995) ○, advection; □, dissipation; ◇, viscous diffusion, △, turbulent diffusion; ▼, pressure–strain; ▲, pressure diffusion.

field of turbulence (e.g. Tennekes & Lumley 1972 or Hinze 1975). For the present application the pressure–strain rate term reduces to the so-called slow pressure–strain rate since there is no mean velocity gradient.

The different terms of the streamwise component of the RST equation at $x/M = 16.2$ are shown in figure 13(*a*). Away from the wall, in the free stream, there is an approximate balance between the dominating advection and the dissipation terms, and this balance seems to prevail down to a wall distance of approximately $x_2/L_{int} = 0.4$. Actually, substantial deviations from this balance are restricted to

the region $x_2/L_{int} < 0.2$. As the wall is approached the pressure–strain and viscous-diffusion terms become of increasing importance while the turbulent diffusion seems to remain small. The advection term tends to zero as the wall is approached. At the wall the dissipation and the viscous diffusion should balance according to the no-slip condition and the continuity equation. This is, however, in a region too close to the surface to be seen from the present measurements.

It is interesting to note that although the wall-normal component is attenuated over a distance of the order of one integral length scale from the wall the active redistribution through the action of the pressure–strain term is restricted to a much thinner region. This is of importance for modelling purposes, in particular for the description of the so-called wall pressure reflection term.

In the thin region where the pressure–strain term is significant, enhanced viscous dissipation and diffusion also contribute to a quite complex scenario. The no-slip condition at the wall gives an enhanced dissipation due to the fluctuating shear components $\partial u/\partial y$ and $\partial w/\partial y$. Close to the wall this effect dominates over the gain from the pressure–strain redistribution in the streamwise and spanwise Reynolds stress components. This situation is, of course, quite different to the case with an 'inviscid' (slip) wall, which also was studied by Perot & Moin. The enhanced dissipation caused by the fluctuating shear in the horizontal velocity components also results in a highly anisotropic dissipation, approaching a two-component state at the wall, i.e. $\varepsilon_{22}/\varepsilon \to 0$ (the uncertainty in ϵ_{11} was estimated to be of the order of 15% based on repeated measurements).

The fact that the pressure–strain rate is practically zero over a substantial region where there is a significant Reynolds stress anisotropy implies that a traditional model for this term, linear (as the Rotta model) or nonlinear, cannot be expected to work without near-wall corrections in this region.

In figure 13(*b*) the DNS data of Perot & Moin (1995) are shown in the same scaling as for the experimental data in figure 13(*a*). It is obvious that due to the physical limitations of the measuring technique the innermost part of the boundary layer cannot be resolved. However, in spite of this, a comparison with figure 13(*a*) shows that all components in the RST equations seem to be very well resolved for x_2/L_{int} larger than 0.1. It is also noteworthy that in our measurements we have obtained the pressure term by balancing the equations, and hence the pressure–strain and pressure diffusion are not separated. From figure 13(*b*), it is obvious that the pressure diffusion term is negligible, and the balanced term shown in figure 13(*a*) represents essentially the pressure–strain rate term.

4.3. *Implications for the near-wall modelling*

The observation that the energy transfer between components is essentially zero over a large part of the 'boundary layer' where the Reynolds stress anisotropy is significant implies a need for near-wall corrections to the traditional models of the slow pressure–strain rate term.

We illustrate the situation by use of the Rotta (1951) model for the slow part of the pressure–strain rate term and as a typical model of wall proximity effects we employ the Gibson & Launder (1978) model. The Rotta model

$$\Pi_{ij}^{(s)} = -c_1 \varepsilon \left(\frac{R_{ij}}{k} - \tfrac{2}{3}\delta_{ij} \right) \tag{4.7}$$

predicts a return to isotropy at a rate influenced by the Rotta constant c_1, usually

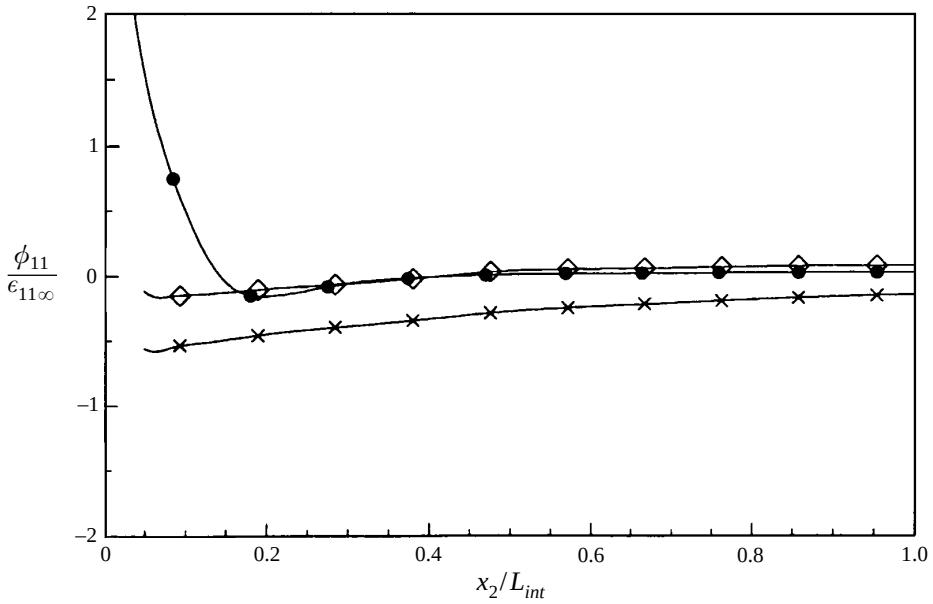

FIGURE 14. Comparison between slow pressure–strain term inferred from measurements and predicted: •, measurement; ⋄, prediction; ×, Rotta contribution.

taken as 1.5–1.8. Here it is assumed that the 'Rotta constant' c_1 varies with Re_T as

$$c_1 = c_R f\,(Re_T) \tag{4.8}$$

where $c_R = 0.8$ and $f\,(Re_T)$ is given by

$$f\,(Re_T) = \frac{B}{40\pi} Re_T \left(\left(1 + \frac{80\pi}{B^2 Re_T} \right)^{1/2} - 1 \right) \tag{4.9}$$

where $B = 0.31$, Hallbäck, Sjögren & Johansson (1993). For the present Reynolds number of about 425 this gives a Rotta constant of approximately 1.4. The Gibson & Launder model

$$\Pi_{ij}^{(\mathrm{w})} = c_1' \frac{\varepsilon}{k} \left(\overline{u_k u_m} n_k n_m \delta_{ij} - \tfrac{3}{2} \overline{u_k u_i} n_k n_j - \tfrac{3}{2} \overline{u_k u_j} n_k n_i \right) f \left(\frac{L_{int}}{x_2} \right) \tag{4.10}$$

which describes the wall damping effect, results in an enhancement of the anisotropy near a wall, where the level of the normal component is decreased by the presence of the wall. The function f is assumed to be directly proportional to L_{int}/x_2, such that $f = 0.4k^{3/2}/\varepsilon$.

Figure 14 shows a comparison between the value inferred from measurements and the predicted value of the pressure–strain correlation, as it appears in the streamwise budget. Also shown is the contribution due to the Rotta term alone. The total dissipation is here determined under the assumption of local axisymmetry. As can be seen the predicted net contribution to $\overline{u_1^2}$ is minor while the measurements indicate a significant contribution in the inner portion of the 'boundary layer'. The absence of a predicted contribution is a reflection of the two counteracting processes as the wall is approached: on the one hand there is the Rotta model acting to reduce the degree of anisotropy and on the other hand we have the Gibson & Launder model acting to

increase the degree of anisotropy. The net result is that the two terms almost cancel each other.

The present experimental results and the numerical simulation results of Perot & Moin (1995) suggest that the strength of the near-wall influence is such as to completely inhibit the pressure–strain redistribution that otherwise would occur over a distance of the order of the integral scale, where the level of anisotropy would indicate a flow of energy from the wall normal to the lateral components. This damping behaviour would be in accordance with typical models of pressure–reflection terms, but the situation is further complicated by the fact that a thinner region exists close to the wall where the pressure–strain indeed transfers energy from the 'energy-poor' wall-normal component to the 'energy-rich' horizontal ones. Hence, the pressure–strain term here tends to increase anisotropy, in contrast to the usual intuitive picture of slow pressure–strain as an 'isotropization term'. This latter part of the damping behaviour is not captured by current models of pressure-reflection effects.

5. Conclusions

Turbulence with a very small degree of anisotropy was generated by applying a small amount of strain to grid-generated turbulence. Measurements of the variances of gradients of fluctuating velocities indicate very small degrees of anisotropy in the small scales as well. By passing this turbulence field over a wall moving at the speed of the free stream we were able to generate a shear-free boundary layer, enabling experimental investigation of wall–turbulence interaction in the absence of mean shear and turbulence production. The initial response of the turbulence field to the insertion of the moving wall was seen to be well described by the theory of Hunt & Graham (1978). The initial transfer from the wall-normal component gives rise to near-wall peaks in the tangential components. For larger downstream distances the Hunt & Graham theory ceases to give an accurate description. In its downstream development the flow field continues, as should be expected, to be roughly axisymmetric with isotropy in planes parallel to the wall. As the downstream distance increases, the initial peaks in the tangential components of Reynolds stress are damped and after an adjustment period corresponding to one to two (macroscale) eddy-turnover times the peaks vanish completely.

In the connection with the damping of the Reynolds stresses the presence of two length scales is evident. This was further illustrated by estimating the different terms of the streamwise RST equation at a station downstream of the initial adjustment region. A complex picture evolves from these results where the near-wall influence gives a damping of the wall-normal component and an inhibition of pressure–strain redistribution over a region extending roughly one integral scale out from the wall. This part of the near-wall influence could be considered to be in accordance with current models of wall proximity effects, which typically assume a wall-distance scaling on $k^{3/2}/\varepsilon$. In a thinner region closest to the wall, though, a much more complicated balance occurs where the pressure–strain actually transfers energy to the horizontal components from the wall-normal one, thus tending to increase the degree of anisotropy. This effect is obviously associated with the change in turbulence structure caused by the presence of the wall, cf. the so-called splatting effect discussed by Perot & Moin (1995). In this region one also finds an enhanced dissipation caused by the fluctuating shear induced by the no-slip condition at the wall. This is also associated with a transport of energy towards the wall.

The near-wall influence in this inner region of the flow is probably quite difficult to capture in one-point closures of standard form, and may require information further to that of the Reynolds stresses, such as e.g. length-scale related quantities.

The authors are grateful to Dr M. Hallbäck at the Royal Institute of Technology in Stockholm for valuable discussions during the course of the work and for the idea of analysing the effect of temperature drift on the measured intensities as it is presented in section 4.1. We are also grateful to Professor I. P. Castro of the University of Surrey for comments on a draft of this paper and to Dr J. Citriniti for comments and various help with the manuscript.

Support from the Swedish Board for Industrial and Technical Development (NUTEK) is gratefully acknowledged.

REFERENCES

Antonia, R. A. & Mi, J. 1993 Corrections for velocity and temperature derivatives in turbulent flows. *Exps. Fluids* **14**, 203–208.

Batchelor, G. K. & Townsend, A. A 1948 Decay of isotropic turbulence in the initial period. *Proc. R. Soc. Lond.* A **193**, 539–558.

Biringen, S. & Reynolds, W. C. 1981 Large-eddy simulation of the shear-free turbulent boundary layer. *J. Fluid Mech.* **103**, 53–63.

Browne, L. W. B., Antonia, R. A. & Shah, D. A. 1988 Selection of wire spacing for X-wires. *Exps. Fluids* **6**, 286–288.

Brumley, B. 1984 Turbulence measurements near the free surface in stirred grid experiments. In *Gas Transfer at Water Surfaces* (ed. W. Brutsaert & G. H. Jirka), pp. 83–92.

Collis, D. C. & Williams, J. 1959 Two dimensional convection from heated wires at low Reynolds numbers. *J. Fluid Mech.* **6**, 357–384.

Comte-Bellot, G. & Corrsin, S. 1966 The use of a contraction to improve the isotropy of grid-generated turbulence. *J. Fluid Mech.* **25**, 657–682.

Corrsin, S. 1963 Turbulence; experimental methods. In *Handbuk der Physik*, vol. V, VII (ed. S. Flügge & C. A. Truesdell). Springer.

Ewing, D. & George, W. K. 1994 Spatial attenuation of vorticity measurements by multi-wire probes. In *Fluid Measurements and Instrumentation. ASME Fluids Division Summer Meeting, Lake Tahoe, Nevada, June 19–23.* FED-Vol. 183.

George, W. K. 1992 The decay of homogenous isotropic turbulence. *Phys. Fluids* **4**, 1492–1509.

Gibson, M. M. & Launder, B. E. 1978 Ground effects on pressure fluctuations in the atmospheric boundary layer. *J. Fluid Mech.* **86**, 491–511.

Groth, J., Hallbäck, M. & Johansson, A. V. 1989 Measurement and modelling of anisotropic turbulent flows. In *Advances in Turbulence II. Proc. Second Eur. Turb. Conf., Berlin September 1988* (ed. H. Fiedler & H. Fernholz), pp. 84–89. Springer.

Hallbäck, M., Sjögren, T. & Johansson, A. V. 1993 Modeling of intercomponent transfer in Reynolds stress closures of homogeneous turbulence. In *Turbulent Shear Flows 9* (ed. F. Durst, N. Kaagi, B. E. Launder and J. H. Whitelaw), pp. 23-4-1–23-4-6. Springer.

Hinze, J. O. 1975 *Turbulence.* McGraw-Hill.

Hunt, J. C. R. & Graham, J. M. R. 1978 Free-stream turbulence near plane boundaries. *J. Fluid Mech.* **84**, 209–235.

Ligrani, P. M. & Bradshaw, P. 1987 Subminiature hot-wire sensors: develpoment and use. *J. Phys.* E: *Sci. Instrum.* **20**, 323–332.

Lueptow, R. M., Breuer, K. S. & Haritonidis, J. H. 1988 Computer-aided calibration of X-probes using look-up tables. *Exps. Fluids* **6**, 115–118.

Perot, J. B. & Moin, P. 1995 Shear-free turbulent boundary layers. Part 1. Physical insights into near-wall turbulence. *J. Fluid Mech.* **295**, 199–227.

Roach, P. E. 1987 The generation of nearly isotropic turbulence by means of grids. *J. Heat Fluid Flow* **8**, 82–92.

Rotta, J. C. 1951 Statistische theorie nichthomogener turbulenz. *Z. Phys.* **131**, 547–572.

Sjögren, T. & Johansson, A. V. 1996 The return to isotropy process in homogeneous, axisymmetric turbulence. Paper to be submitted.

Smits, A. J. & Perry, A. E. 1981 A note on the hot-wire anemometer measurements of turbulence in the presence of temperature fluctuations. *J. Phys.* E*: Sci. Instrum.* **14**, 311–312.

Tennekes, H. & Lumley, J. L. 1972 *A First Course in Turbulence*. MIT Press.

Thomas, N. H. & Hancock, P. E. 1977 Grid turbulence near a moving wall. *J. Fluid Mech.* **82**, 481–496.

Wyngaard, J. C. 1968 Measurement of small-scale turbulence structure with hot-wires. *J. Phys.* E: *Sci. Instrum.* **1**, 1105–1108.

Wyngaard, J. C. 1969 Spatial resolution of the vorticity meter and other hot-wire arrays. *J. Phys.* E: *Sci. Instrum.* **2**, 983–987.

Uzkan, T. & Reynolds, W. C. 1967 A shear-free turbulent boundary layer. *J. Fluid Mech.* **28**, 803–821.